frontiers | Frontiers in Earth Science

TYPE Original Research
PUBLISHED 13 March 2023
DOI 10.3389/feart.2023.1136012

OPEN ACCESS

EDITED BY
Muhammad Aleem Zahid,
Lasbela University of Agriculture, Water and Marine Sciences, Pakistan

REVIEWED BY
Zheng Cao,
Chongqing University of Science and Technology, China
Changcheng Han,
Xinjiang University, China
Muhammad Jawad Munawar,
University of the Punjab, Pakistan

*CORRESPONDENCE
Cunfei Ma,
mcf-625@163.com

SPECIALTY SECTION
This article was submitted to Solid Earth Geophysics, a section of the journal Frontiers in Earth Science

RECEIVED 02 January 2023
ACCEPTED 20 February 2023
PUBLISHED 13 March 2023

CITATION
Fang Z, Zhang L and Ma C (2023), Development and controlling factors of shale lithofacies cycles in a continental rift basin: A case study of Es_4^u in the Boxing Subsag of Dongying Sag, Bohai Bay Basin, China.
Front. Earth Sci. 11:1136012.
doi: 10.3389/feart.2023.1136012

Development and controlling factors of shale lithofacies cycles in a continental rift basin: A case study of Es_4^u in the Boxing Subsag of Dongying Sag, Bohai Bay Basin, China

Zhengwei Fang[1,2,3,4,5], Liqiang Zhang[1] and Cunfei Ma[1]*

[1]School of Geosciences, China University of Petroleum (East China), Qingdao, China, [2]Research Institute of Petroleum Exploration and Development, Sinopec Shengli Oilfield Company, Dongying, China, [3]Sinopec Key Laboratory of Shale Oil/Gas Exploration and Production, Shengli Oilfield Branch, Dongying, China, [4]Shandong Provincial Key Laboratory of Unconventional Oil and Gas Exploration and Development, Dongying, China, [5]Key Laboratory of Sedimentary Simulation and Reservoir Evaluation, Sinopec Shengli Oilfield Company, Dongying, China

The shale of the upper Es4 formation (Es_4^u), deposited during the Eocene in the Boxing Subsag of the Dongying Sag, is a typical set of lime-rich lacustrine shale in a continental rift basin. Through logging data interpretation, core and thin section observations, and geochemical elements [obtained by X radial fluorescence (XRF) mud logging] analysis, the development and controlling factors of lithofacies cycles of Es_4^u shale were analyzed. The results show that 22 types of lithofacies with typical characteristics are developed in Es_4^u, indicating the sedimentary environments, such as lower lakeshore (LL) slope zone; upper, middle, and lower shallow-lake slope zones; semi-deep-lake zone; and deep-lake zone. Lithofacies cycles in three scales are recognized in Es_4^u: small-scale lithofacies cycles indicated by alternate development of two lithofacies, mesoscale lithofacies cycles indicated by the repetition of lithofacies associations or regular variation of multiple lithofacies, and large-scale lithofacies cycles indicated by regular variation of well logging curves, which have the average thickness of approximately 0.4, 5, and 35 m, respectively. According to the vertical variation of astronomical parameters and lithofacies cycles, the periodic change in long eccentricity has a close relationship with the large-scale lithofacies cycle, the periodic change in slope is closely relative to the mesoscale lithofacies cycle, and the periodic change in precession is closely related to small-scale lithofacies cycle. However, the periodic change in short eccentricity correlates poorly with lithofacies cycles. The climate change reflected by long eccentricity and slope is quite distinct from the actual basin climate reflected by the paleoclimatic parameters (e.g., Rb/Sr and Sr/Cu), indicating that the basin paleoclimate was greatly influenced by the paleogeological conditions. For shale in Es_4^u of the Boxing Subsag, approximately 55% of the shale stratigraphic record is dominantly controlled by the astronomical climate and 45% by the paleogeological conditions. Affected by the paleogeological conditions, large-scale and mesoscale lithofacies cycles are different in lithofacies types and superimposition patterns, and just small-scale lithofacies cycles are found repetitive vertically. These findings suggest that the lithofacies cycles of shale in a continental rift basin are a product of astronomical driving mechanism

(Milankovitch forcing) and variation of local paleogeological conditions, which is apparently different from the sedimentary record of marine shale that is evidently controlled by the Milankovitch cycle. Therefore, the lithofacies cycles should be comprehensively analyzed under the background of actual basin paleoclimate.

KEYWORDS

continental rift basin, shale, lithofacies type, lithofacies cycle, development characteristic, controlling factor

1 Introduction

"Cycle" is an important feature of the stratigraphic record, and a cyclical stratigraphic record is the product of a sedimentary cycle, sedimentary environment, or driving mechanism (Gong et al., 2008). Cyclostratigraphy and high-resolution sequence stratigraphy enable us to find out that marine sediment cycles are controlled by the regular changes in orbital parameters (e.g., eccentricity, obliquity of the ecliptic, and precession) of the Earth, which lead to global climate changes, accompanied by the synergistic changes in sea level and sedimentary facies (Kitamura, 1997; Gale et al., 2002; Kukla, 2005; Ridente et al., 2009; Ridente and Lobo, 2014). Compared with the sea level, the lake level of continental basins is sensitive to not only the orbital parameters globally but also to the basin climate and tectonic activities regionally. They present more intense fluctuation and complex frequency changes and induce more diverse and frequent vertical variables of sedimentary lithofacies. For example, the shales of Es_4^u and Es_3^l in the Jiyang Depression, with thicknesses of 300–600 m, contain dozens of types of lithofacies (Wang et al., 2016). Obvious lithofacies cycles can be observed at some intervals of the core but are unstable and variable vertically. The present results show that the typical Milankovitch cycle exists in many lacustrine deposits (Szurlies, 2007; Machlus et al., 2008; Abels et al., 2009; Walters et al., 2020). The Milankovitch cycle was also found in some continental deposits in China, such as the Late Cretaceous in the Songliao Basin (Wu et al., 2014) and the Middle Permian Lucaogou and Jingjingzigou formations and Late Triassic Yanchang Formation in the Ordos Basin (Zhang et al., 2019; Olariu et al., 2022). In the Jiyang Depression of the Bohai Bay Basin, the cyclical sedimentary records of the Paleogene Kongdian Formation include color meter-scale cycle, graded meter-scale cycle, and non-graded meter-scale cycle, which have been proved to be controlled by the Milankovitch cycle (Tan et al., 2015). In the Dongying Sag of the Jiyang Depression, an intact Milankovitch cycle was found in the Paleogene shale strata, and it is believed to have been deposited mainly under the control of long eccentricity and precession (Sun et al., 2017; Shi et al., 2019; Shi et al., 2020).

The previous studies have demonstrated a broad consensus on the development of the Milankovitch cycle in fine-grained continental sediments and marine sediments. However, besides the driving of astronomical mechanisms, some other driving mechanisms impact these sediments. Ito et al. (1999) found that local basin tectonics can be an important forcing mechanism of high-frequency depositional sequences in Pleistocene successions in an active-margin basin. Colombié et al. (2012) revealed that marl–limestone alternations in the Late Jurassic period of western France resulted from the combined effects of cyclic changes in carbonate production and high-energy, episodic events. Victorien et al. (2019) reported that the vertical and lateral variability of the LBG (Lower Barrow Group, developed in the Northern Carnarvon Basin on the North West Shelf of Australia) resulted from variations in sediment supply and subsidence regime under local (i.e., process regime and currents), regional (i.e., tectonics), and global (i.e., eustasy and climate) forcing parameters interplaying across timescales. For lacustrine fine-grained sediments, current studies rarely discussed the impact of basin-domain paleogeological conditions on the lithofacies cycle. A deep analysis of lithofacies cycles under the control of various mechanisms is important to improve the understanding of the depositional environments and sedimentary processes, reveal the genesis of lithofacies and its cycles, and predict the distribution of lithofacies. Moreover, the types and scales of cycles under the joint control of the astronomical mechanism and basin-domain characteristics need further investigation. The lithofacies type affects not only the shale reservoir performance (Iqbal et al., 2021; Shu et al., 2021; Woo et al., 2021) but also the fracture characteristics, which is directly related to the target layer selection of shale oil horizontal well and design of the hydraulic fracturing scheme.

In this paper, by integrating core observation, thin section analysis, X-ray fluorescence (XRF) element scanning, and well logs, taking shales in the upper submember of the fourth member of Eocene Shahejie Formation (Es_4^u) of Boxing Subsag for research object, the compositions, scales, and controlling factors of lithofacies cycles are analyzed and discussed. It aims to present a novel approach to understanding the relationship between the lithofacies and astronomical cycles (Milankovitch cycle) and provide theoretical support to the prediction of favorable lithofacies with shale oil exploration in continental rift basins.

2 Geological setting

The Dongying Sag is a secondary structural unit in the Jiyang Depression of the Bohai Bay Basin, China (Figure 1A). As a typical half-graben lacustrine basin during the Paleogene, the Dongying Sag spreads along the northeast and neighbors the Qingtuozi Uplift in the east, the Qingcheng Uplift in the west, the Guangrao Uplift and Luxi Uplift in the south, and the Chenjiazhuang Uplift and Binxian Uplift in the north (Figure 1B). It is approximately 90 km long from east to west and 65 km wide from south to north, covering an area of 5,700 km^2. It includes four subsags: Minfeng, Lijin, Niuzhuang, and Boxing (Zhang et al., 2020; Wang et al., 2021). The Boxing Subsag is located in the southwestern part of the Dongying Sag. In Boxing Subsag, a huge set of lacustrine shales is developed from the upper member of the Fourth Shahejie Formation (Es_4^u) to the lower

10.3389/feart.2023.1136012

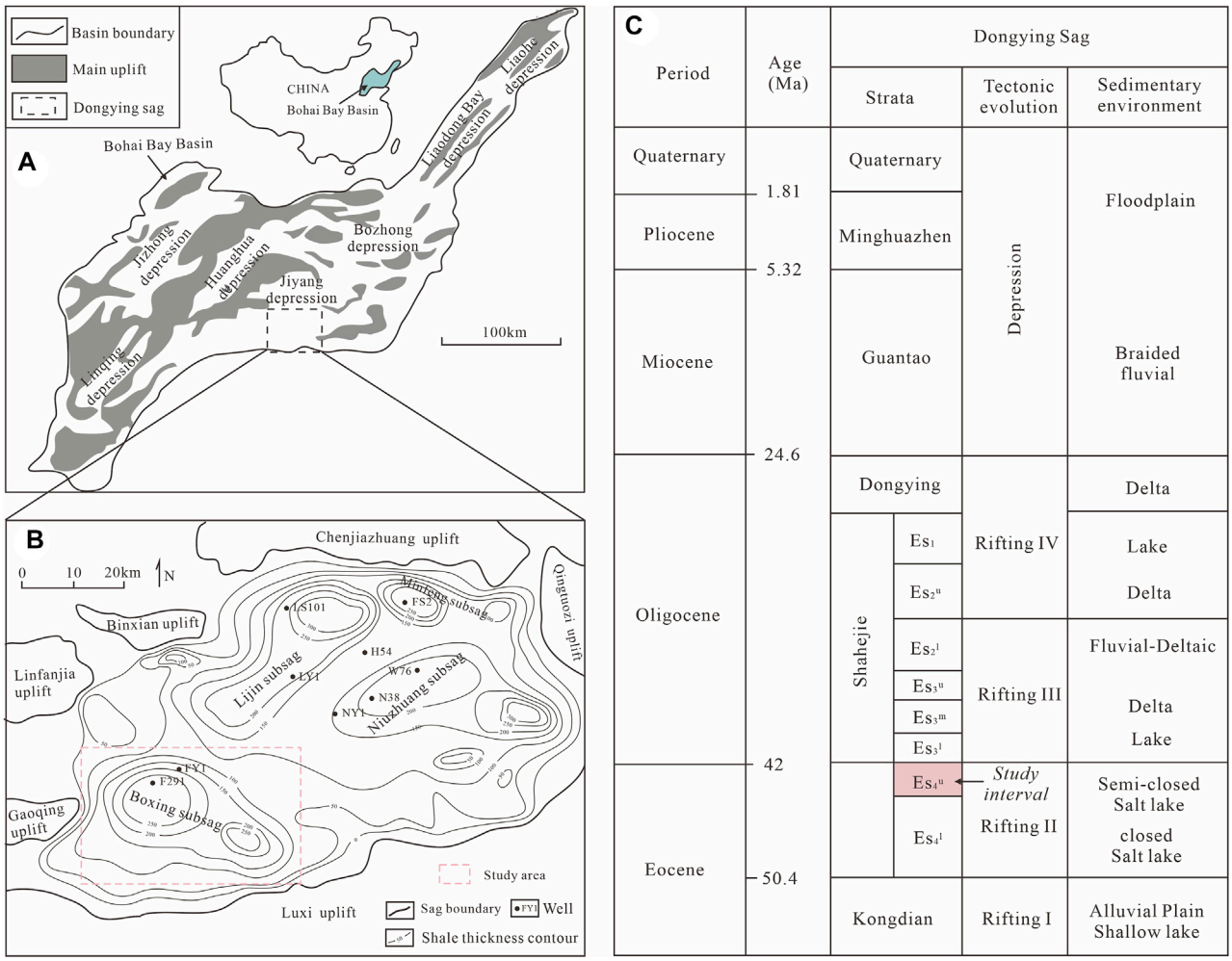

FIGURE 1
(A) Location, **(B)** shale thickness and well distributions, and **(C)** stratigraphic column of Dongying Sag (quoted and modified from Zhang et al., 2020).

member of the Third Shahejie Formation (Es_3^l) of Eocene, which is the major source rock. During the deposition of Es_4^u, the lake water was highly saline for the prosperity of halophilic microorganisms. The lake water existed in stable layers depending upon salinity and density. The bottom layer was in an H_2S-rich strong reducing condition favorable for organic matter preservation, thus forming dark gray-to-gray-black shales of brackish–salified lake, with a thickness of 200–300 m (Sun et al., 2017; Wang et al., 2019) and well-developed laminae. According to the X-ray diffraction (XRD) analysis of core samples from Es_4^u, the shale is rich in carbonates, including terrigenous clasts and clay minerals (3%–96%, avg. 49%), and chemical components (4%–97%, avg. 51%) and contains multiple types of lithofacies (Song, 2019). Thus, the Es_4^u shale is a typical object for lithofacies cycle research.

3 Materials and methods

FY1 is a well with a continuous core in Es_4^u (from 3,245 to 3,440 m) of Boxing Subsag, which is considered geographically representative of the entire territory of the Boxing Subsag and selected for the study. A total of 753 core samples were obtained about 0.25 m and divided into multiple parts. A total of 753 thin sections were made for the identification of rock composition and microstructure. The mineral composition of the rocks was investigated using XRD from one part of the 753 core samples. In addition, 100 core samples were used for inductively coupled plasma (ICP) analysis and obtained the element composition of the rocks. Thin section identification, XRD, and ICP analysis were conducted in Sinopec Key Laboratory of Shale Oil/Gas Exploration and Production, Shengli Oilfield Branch. D/max-2500PC diffractometer was used for XRD analysis, and IRIS IntrepidII XSP was used for ICP analysis.

Typical components and sedimentary structures of shale were recognized based on core observation and thin-section identification, which can reflect the characteristics of the sedimentary environment.

The well logging data of Well FY1 were used in this study to analyze lithofacies cycles of different scales. There are 820 sampling points in Es_4^u of Well FY1, 3,240–3,445 m, with a sampling interval

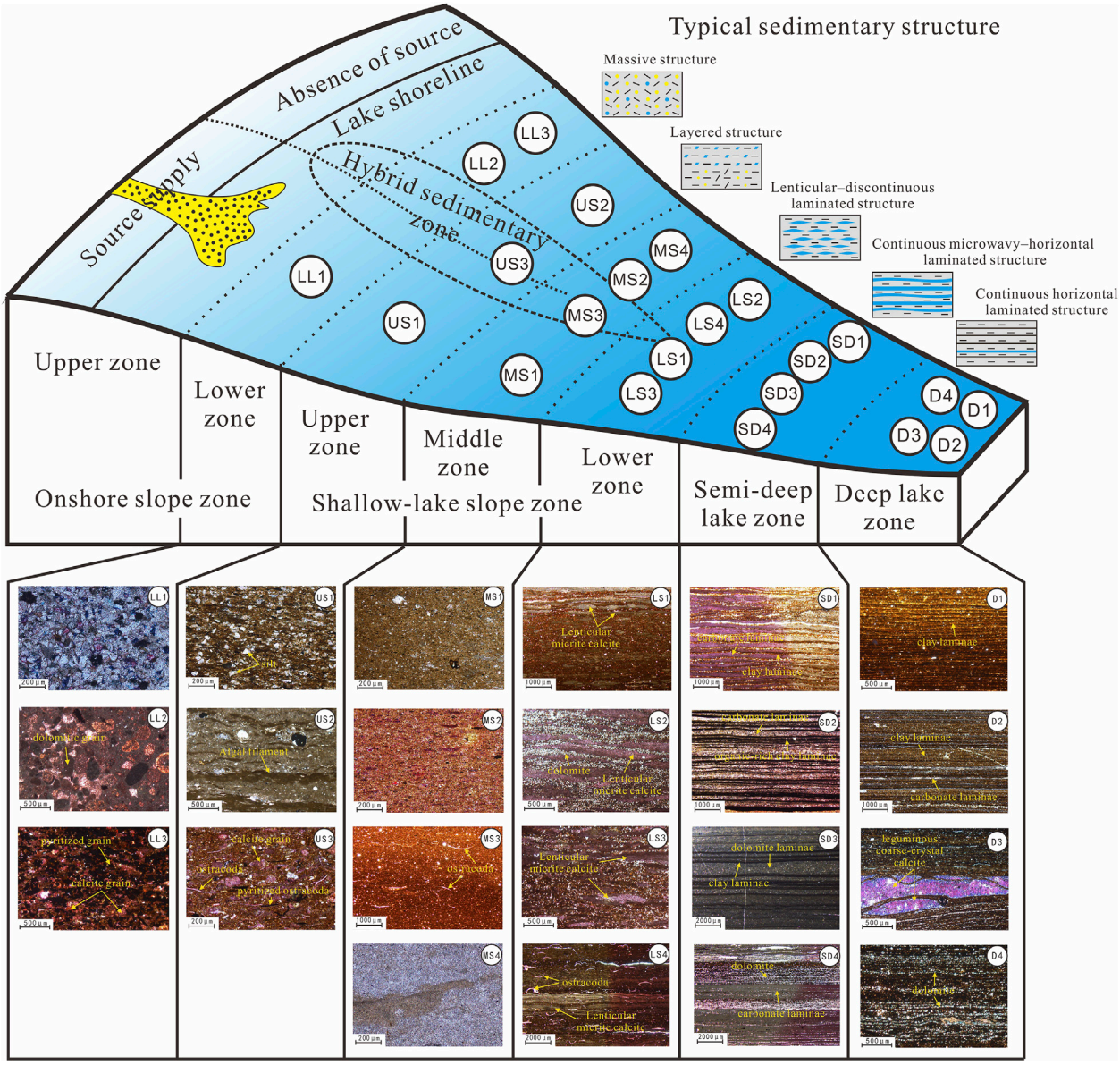

FIGURE 2
Types and distribution of lithofacies in Es_4^u of Boxing Subsag.

of 0.125 m. Among well logging data, the Th log in natural gamma-ray (GR) spectral logging was selected for astronomical cycle analysis; the natural GR logging and 0.4 m gradient resistivity (R4), which are sensitive to shale lithology and lithofacies, were selected for large scale cycle identification. All logging data were normalized by Shengli Logging Company before being obtained.

In order to obtain high-resolution element composition to identify medium and small-scale lithofacies cycles, an X-ray fluorescence (XRF) spectrum scanner was used. By testing the strength of the output signal, a portable XRF spectrum scanner (XRF) can qualitatively and semi-quantitatively analyze the chemical element composition and obtain high-resolution continuous element records of sediments, which has the advantages of being less destructive, convenient, and fast and has been widely used to study sedimentary paleoenvironment changes of sediments in lake, ocean, river, and loess sedimentation (Tian et al., 2011; Walters et al., 2020). In this study, the hand-held XRF spectrometer produced by Bruker Company was used on the core section of FY1, 3,240–3,445 m. The general mode was selected for the test. The detection voltage was 10 kV, the current was 0.15 mA, the detection time was 60 s, and the sampling interval was 4–15 cm. A total of 2,334 data points were obtained, and major elements (e.g., Ca, Si, Al, Mg, Fe, and K) and trace elements (e.g., Ti, Rb, Cr, Mn, Sr, P, Cu, and Zr) were detected, more than 20 species. All element data obtained from XRF completed normalized processing in Origin 9.0.

4 Results

4.1 Types and characteristics of typical lithofacies

Identification of lithofacies types is the basis of lithofacies cycle research. Recent studies have shown that the shales in the Jiyang Depression can be divided into three categories: 1) laminated, with single-lamina thickness <1 mm; 2) layered, with single-layer thickness ≥1 mm; and 3) massive, generally with no oriented components observed on thin sections, according to the rock composition, sedimentary structure, lime texture, and organic matter abundance (Wang et al., 2016). However, there is no consensus on the origin and sedimentary environment of each type of lithofacies. In this study, through core and thin section observations of shale samples from Es_4^u in the Boxing Subsag, 22 types of typical lithofacies were identified depending on sedimentary components and structures (Figure 2). These typical lithofacies can effectively reflect the relative position of lake level and sedimentary facies belt in the deposition period and are described in detail in the following sections.

4.1.1 Lithofacies types of the lower lakeshore (LL) slope zone

Massive/layered silty-fine sandstone (LL1) has a massive or layered structure and granular texture. The clastic particles are mainly very fine sands and a small amount of silt. The clastic components are mainly quartz and feldspar, as well as a small amount of mica, fragments of crystalline rock, and carbonatite. The intergranular fillings are clay minerals, dolomite, and calcite. This type of lithofacies indicates a relatively low lake level and sufficient sediment supply. It is formed by mechanical transportation. Sufficient terrigenous clastics are transported by the bottom flow from the lakeshore slope to the lake and finally subside with the gradual decline of water energy.

Massive/layered cryptocrystalline granulated dolomite (LL2) and granulated limestone (LL3) have a massive or layered structure and granular texture, which comprises dominant sand-size grains and partial silt-size grains. The grains include cryptocrystalline dolomitic and limy silt to sand-sized allochem, oolites, and bioclasts, and a certain number of terrigenous clasts. This type of lithofacies indicates a salified sedimentary environment with a relatively low lake level and an insufficient sediment supply. The dolomitic or limy soft mud at the bottom of the lakeshore zone is broken and washed under the wave action and reprecipitated to form this lithofacies type. The granulated limestone is deposited in a water body with a salinity lower than that of the granulated dolomite.

4.1.2 Lithofacies types of the upper shallow-lake (US) slope zone

Layered silty mudstone-muddy siltstone (US1) has mainly layered structure and partially laminated structure, with relatively straight bedding boundary or lamina boundary. The main components are silt and mud; silt is mixed with mud. This type of lithofacies is formed under sufficient sediments, transported by low-density laminar flow, and then unloaded and deposited in the gentle lower slope zone of the shallow lake.

Layered algal-remains-bearing muddy cryptocrystalline dolomite (US2) has a layered structure and is mainly composed of dolomite, calcite, and mud, as well as a small number of terrigenous clasts. Mud is uniformly mixed in dolomite. Deformed algal bands and tubular algal remains completely filled with single-crystal calcite are observed. This type of lithofacies is formed under the joint action of biological and chemical precipitations in the benthic algae zone of the shallow-lake slope.

Layered Ostracoda-bearing muddy cryptocrystalline limestone (US3) has a layered structure and is mainly composed of grains, calcite, mud, and some silts. The grains are mainly ostracod fragments and a small amount of microcrystalline–cryptocrystalline limy algal remains. The ostracod fragments show significant directional arrangement. This type of lithofacies is formed by frequent biological and mechanical processes. After the death of ostracods, they are buried together with limy soft mud in the Ostracoda development zone of the shallow-lake slope.

4.1.3 Lithofacies types of the middle shallow-lake (MS) slope zone

Layered mudstone (or MS1) has a layered structure and muddy texture. It is mainly composed of mud, with a small amount of silt, and oriented ostracod fragments occasionally. This type of lithofacies is formed by mud flocculation. Mud from the provenance is slowly deposited under flocculation.

Layered cryptocrystalline limestone (MS3) and dolomite (MS4) have a layered structure. They are composed of cryptocrystalline lime or dolomite, with a small amount of mud. They are generally homogeneous and not subject to evident hydrodynamic action. This type of lithofacies is formed by chemical precipitation in the shallow lake, with a relatively saline water body and lack of sedimentary source.

Layered ostracod-bearing and silt-bearing mudstone (MS3) has a layered structure and muddy texture. It is mainly composed of mud, with some silts and ostracod fragments. The ostracod fragments are oriented along the bedding. This type of lithofacies is deposited below the normal wave base in the shallow-lake zone, with occasional wave action and sufficient sediment supply. The lake water is quiet, and the sediments bring rich nutrients, suitable for the growth of benthic Ostracoda.

4.1.4 Lithofacies types of the lower shallow-lake (LS) slope zone

Lenticular laminated limestone mudstone (LS1) has a lenticular structure. The micritic or powder crystal limes are lenticular, banded, and wrapped by mud; the mud mixes with a small amount of silt. This type of lithofacies is formed by uneven plane distribution and temporal alternation of mud flocculation and chemical sedimentation in the lower shallow-lake slope zone, with insufficient sediment supply.

Lenticular laminated dolomite limestone (LS2) has a lenticular structure. The micritic or powder crystal limes are lenticular, banded, and wrapped with clay and dolomite. Dolomite displays a crystal texture with uniform crystal size. The sedimentary facies belt of this lithofacies type is consistent with the lenticular laminated limestone mudstone, but it is deposited in a saltier water body. The alternating precipitation of limy and dolomitic lamina indicates the alternating change of water salinity.

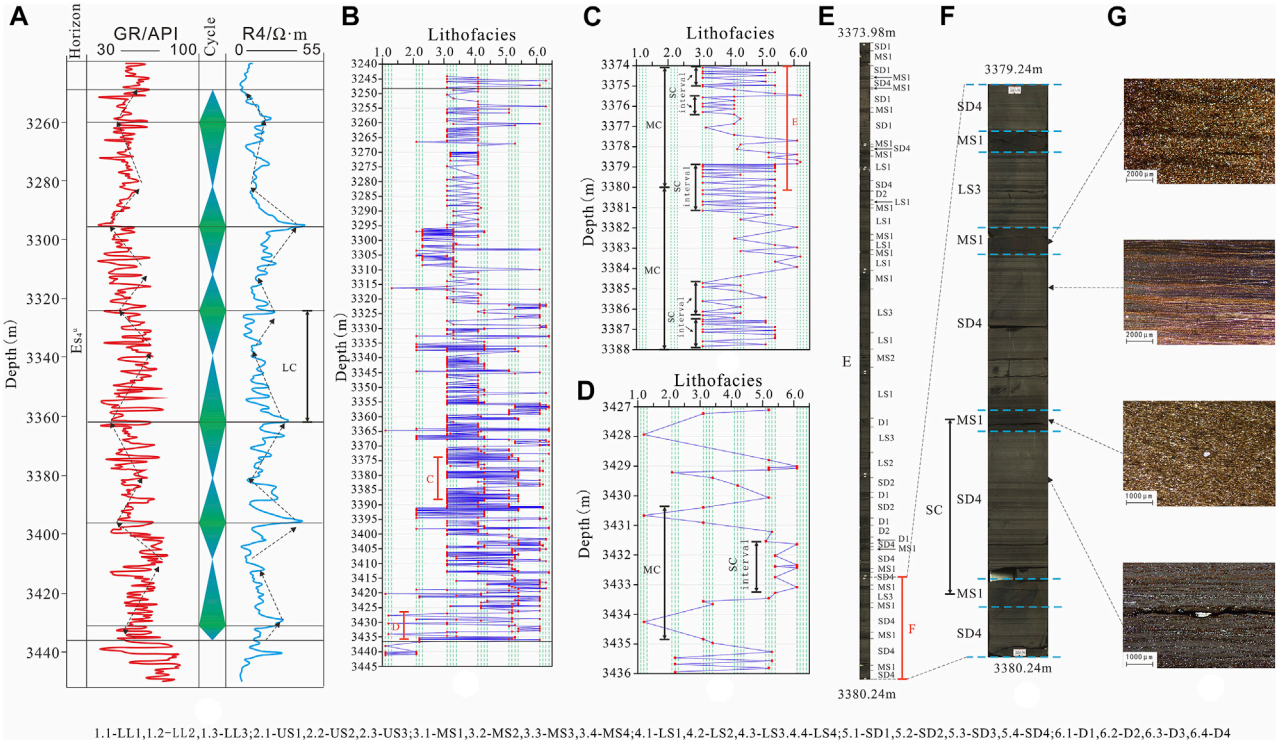

FIGURE 3
Different scales of lithofacies cycles in Es_4^u in Boxing Subsag: large-scale lithofacies cycle **(A)**, vertical lithofacies change **(B)**, typical mesoscale lithofacies cycle **(C–E)**, typical small-scale lithofacies cycle **(F)** and thin-section Images in F **(G)**.

Lenticular/imbricate lime–silty–muddy peperite (LS3) has a lenticular structure. The micritic or powder crystal limes are lenticular, banded, and filled with or wrapped with mud and silt. This type of lithofacies is formed in the environment with frequent alternation of mechanical and chemical sedimentation processes in the shallow-lake zone, with unstable sediment supply.

Lenticular ostracod-bearing limestone mudstone (LS4) has lenticular lamina. The micritic or powder crystal limes are lenticular, banded, and wrapped with mud; the mud mixes with a small amount of silt. Some oriented ostracod fragments are observed. This type of lithofacies is formed under the temporal alternation of mud flocculation, chemical sedimentation, and biological action in the lower shallow-lake slope zone, which is suitable for the growth of ostracods and insufficient in sediment supply.

4.1.5 Lithofacies types of the semi-deep-lake (SD) zone

Laminated muddy cryptocrystalline limestone (SD1) and dolomite (SD3) have a laminated structure with fine and straight laminae. The lamination is mainly displayed as the interbedding of the organic-rich clayey lamina and limy lamina or dolomitic lamina. The laminae are evenly distributed with a clear boundary. The thickness of the lamina is 0.05–0.15 mm in general. The limes and dolomites are micritic or powder crystal textures. The laminae are formed by the repetitive supply of carbonate and clayey components frequently and periodically. As a result of the alternation of seasonal periodic biochemical and mechanical actions in the semi-deep-lake zone, the carbonate components are deposited under the biochemical actions in summer and autumn, and the clayey components are deposited under the action of flocculation in winter and spring (Liu and Zhou, 2007).

Laminated muddy sparite limestone (SD2) has the same structure and composition as SD1. However, it differs from SD1 in the limy laminae with medium-to-fine crystal texture and a higher organic matter content in the interbedded clayey laminae. The medium-to-fine crystal limy laminae are recrystallized with micritic limy lamina.

Laminated dolomitic muddy cryptocrystalline limestone (SD4) has a laminated structure. There are mainly three types of laminae: limy lamina, clayey lamina, and dolomite mitochondrial lamina, showing uneven thickness and distribution. This type of lithofacies is deposited in a saltier water body than that in SD1, and different laminae indicate the frequent change in water salinity.

4.1.6 Lithofacies types of the deep-lake (D) zone

Laminated organic-rich mudstone (D1) has a laminated structure and is mainly composed of clay minerals. The lamination is displayed as the interbedding of the clayey and organic laminae, and the bedding boundary or lamina is straight. This type of lithofacies is formed by the alternation of sedimentation of dead planktons and mud flocculation in a quiet water body of deep-lake.

Laminated lime-bearing mudstone (D2) has a laminated structure. The lamination is displayed as the interbedding of the clayey and organic laminae, with a small amount of cryptocrystalline

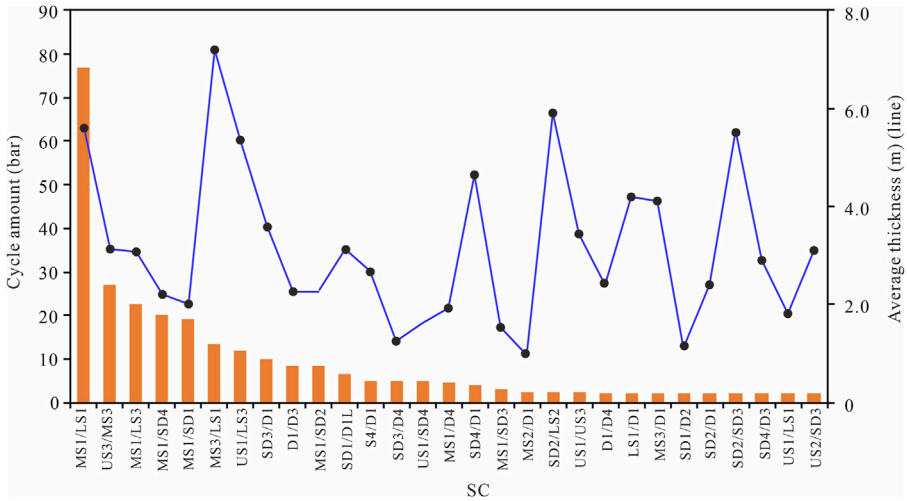

FIGURE 4
Amount and average thickness of SCs in Es_4^u of Well FY1.

limy lamina that is unevenly distributed between the former types of laminae. This type of lithofacies is deposited in a similar process to D1, except for the occasional chemical precipitation, which results in uneven distribution of limy lamina.

Laminated mudstone containing sparry calcite (D3) has a similar structure to D1, but it differs from D1 in the distribution of leguminous coarse crystal calcite locally and chain-shaped fine crystal calcite along the lamina. Both leguminous and chain-shaped calcites are formed during diagenesis, reflecting that this type of lithofacies is deposited in a saltier water body than that in SD1. The sedimentary facies belt of D3 is considered deep-lake according to the fine and straight laminae.

Laminated dolomitic mudstone (D4) has a laminated structure. The bedding is mainly displayed as the dolomite mitochondrial lamina. The dolomite presents a fine crystal and micritic texture and develops densely in mitochondrial form, with some organic matter and clayey lamina therein. This type of lithofacies corresponds to a deep-lake sedimentary facies belt and is deposited in a relatively salty water body. The clay is rich in magnesium ions during deposition, which is gradually precipitated to form mitochondrial dolomite during burial.

4.2 Types and characteristics of lithofacies cycles

Different types of lithofacies of shales show shade variation on the core sections owing to different components and textures. The vertical stacking characteristics of lithofacies were investigated based on the cores, thin sections, and well log curves of Well FY1. The results show that the shale lithofacies in Es_4^u develop in three scales of cycles: small-scale lithofacies cycle indicated by alternate development of two lithofacies (Figures 3E–G), mesoscale lithofacies cycle indicated by the repetition of lithofacies associations or regular variation of multiple lithofacies (Figures 3C, D), and large-scale lithofacies cycle indicated by regular variation of well logging curves (Figure 3A).

4.2.1 Small-scale lithofacies cycle indicated by alternate development of two lithofacies (SC)

According to the core section observation and analysis, small-scale lithofacies cycle in the Es_4^u of Boxing Subsag are found, mainly indicated by the alternate development of two types of lithofacies (Figures 3E, F). The result of thin section identification shows that lithofacies with the same color and bedding structure have relatively consistent mineral components (Figure 3G). Statistics show that 29 types of SC and 276 SCs can be recognized (Figure 4), among which the quantity of eight types of SC is more than or equal to 10, namely, MS1/LS1 (77), US3/MS3 (27), MS1/LS3 (22), MS1/SD4 (20), S1/SD1 (19), MS3/LS1 (13), US1/LS3 (12), and SD3/D1 (10), with the average thickness of 0.56, 0.31, 0.31, 0.22, 0.20, 0.72, 0.53, and 0.36 m, respectively (Figure 4). On the whole, the thickness of a single SC is 0.02–2.28 m, mostly less than 0.6 m, with an average of approximately 0.4 m (Figure 5). The thickness of SC is 106 m, accounting for 56% of the total core thickness (approximately 186 m).

4.2.2 Mesoscale lithofacies cycle indicated by the repetition of lithofacies associations or regular variation of multiple lithofacies (MC)

Based on the recognition of SC, a systematic analysis was conducted on the vertical lithofacies association. It is found that there are mesoscale cycles of lithofacies indicated by the repetition of lithofacies associations in Es_4^u in the Boxing Subsag. For example, in Figure 3C, MS1/SD4 is repeated vertically, and in Figure 3D, LL2-SD4/D1-LL2 changes regularly vertically, showing great fluctuations in lake level. A total of 37 MCs can be identified in Es_4^u of the Boxing Subsag. Owing to the complex variation of lithofacies associations, almost no two MCs have the same superimposition of lithofacies (Table 1). The thickness of MCs in Well FY1 is approximately 2–13 m, with an average of approximately 5 m (Table 1). Specifically, statistics show that the MCs with a thickness of 3–4 m showed the most development, followed by those with a thickness of 2–3 m, 5–6 m, 6–7 m, and 4–5 m. MCs with other thickness ranges showed less development (Figure 6).

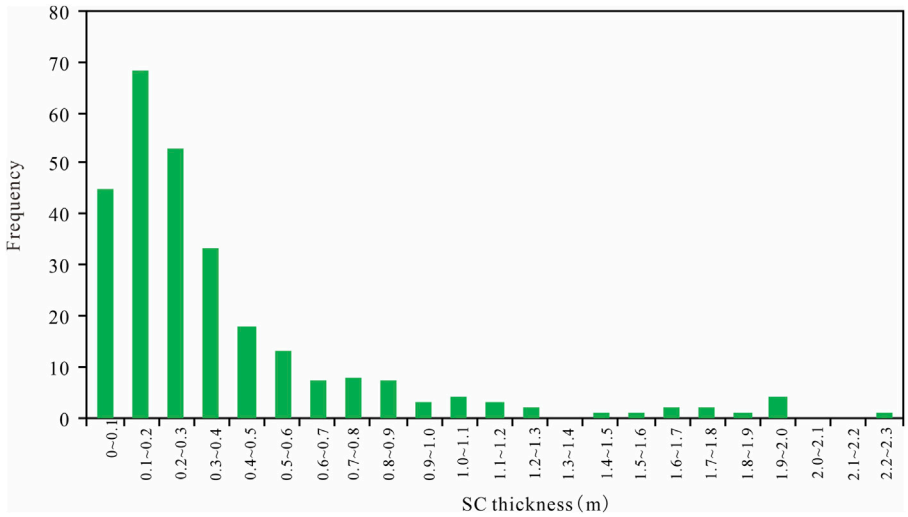

FIGURE 5
Frequency histogram of SC thickness in Es_4^u of Well FY1.

4.2.3 Large-scale lithofacies cycle indicated by regular variation of well logging curves (LC)

Logging response is a macroscopic feature of lithofacies change. The analysis of logs of Well FY1 indicates that GR and R curves change consistently and cyclically. GR is the most effective logging curve for identifying lithology. Deep and shallow resistivities show basically no change in amplitude difference and can effectively reflect the changes in rock components. Thus, it is reasonable to use the changes in GR and R curves to indicate the vertical variation of lithofacies or lithofacies associations. The inflexion point of change can be used as the interface to divide the lithofacies associations. In the study area, the increasing GR and decreasing R are the responses of increasing clay components, whereas the decreasing GR and increasing R are the responses of increasing carbonate components. According to GR and R variations, the Es_4^u in Well FY1 can be divided into five relatively complete cycles of low GR/high R to high GR/low R to low GR/high R, one semi-cycle of low GR/high R to high GR/low R, and one semi-cycle of low GR/high R to high GR/low R (Figure 3A). The thickness of a complete LC is 30–40 m or 35 m on average.

5 Discussion

The analysis of controlling factors of the lithofacies cycle has always been the key issue in the field of lacustrine shale research, which is important for us to restore the filling process of the basin and predict and utilize the basin resources. In a continental rift basin, lithofacies cycles should be the product of stack responses of global and local controlling factors, both of which have an important impact on the development of lithofacies cycles. The global controlling factor is mainly the regular change in astronomical parameters, whereas local controlling factors include the climate and tectonic activity of the basin. This paper analyzes the controls of the astronomical driving mechanism and local paleogeological conditions on different scales of lithofacies cycles. Because Boxing Subsag is located in the gentle slope of the Dongying Sag, the tectonic activities have little impact on the sedimentation of this area, which is not discussed here.

5.1 Driving effect of the astronomical mechanism (Milankovitch cycle)

As described in the Introduction section, the Milankovitch cycle is universal in lacustrine sediments. It is crucial to elucidate how the Milankovitch cycle controls different scales of lithofacies cycles and whether it is consistent with the actually identified lithofacies cycles to clarify the control of the astronomical mechanism. According to Tan et al. (2015), the control of the Milankovitch cycle on a stratigraphic cycle should be determined by reckoning whether the stratigraphic cycle conforms to the period of the Milankovitch cycle and whether the chemical element composition is intrinsically related to the climate effect of the Milankovitch cycle, that is, whether the thickness of the lithofacies cycle is consistent with the formation thickness at the deposition rate controlled by astronomical orbital parameters and whether the climatic characteristics controlled by astronomical orbital parameters are closely related to the paleoclimatic characteristics revealed by geochemical elements. The content of the Th element in sedimentary rocks can effectively reflect the content of clay minerals, which come from the terrigenous area and are closely related to weathering under paleoclimatic conditions, so it is one kind of sensitive element to paleoclimate and can be used to analyze the Milankovitch cycle of sedimentary strata (Li et al., 2019). The Milankovitch cycle analysis of Es_4^u in the Boxing Subsag was conducted using the Th log from the natural GR spectral logging to avoid using the same element data obtained from XRF. The Th log exhibits good continuity (sampling interval of 0.125 m) and reliability. It also can be compared with the paleoclimatic

10.3389/feart.2023.1136012

TABLE 1 Superimposition of lithofacies within MCs and their thicknesses.

No.	Cycle top	Cycle bottom	Superimposition of lithofacies within MC	Thickness (m)
1	3,250.65	3,258.89	MS1/LS1-MS1/SD1-LS1-D3-LS1-MS1/LS1	8.24
2	3,258.89	3,266.76	US1-MS1/LS1-SD3-D1-MS1/LS1	7.87
3	3,266.76	3,275.09	MS1/LS1-MS2/LS1-SD3-US1	8.33
4	3,275.09	3,288.41	MS1/LS1-MS3/LS1-MS1/LS1	13.32
5	3,288.41	3,297.89	US3/MS3-MS1/LS1-MS3/LS1-MS1/LS1	9.48
6	3,297.89	3,305.47	US1/US3-US1/MS3-MS3/D1-US3/MS3	7.58
7	3,305.47	3,311.81	MS2-LS1-D1-US3/MS3-US3/MS1-US1/US3	6.34
8	3,311.81	3,316.48	LL3-MS1/LS1-MS2	4.67
9	3,316.48	3,320.10	MS1/LS1-MS3-LL3	3.62
10	3,320.10	3,324.55	LS1-LS3-SD3/D1-D1/D3-MS3/LS1-MS1/LS1	4.45
11	3,324.55	3,327.70	MS1-SD3/D1-LS3-LS1	3.14
12	3,327.70	3,332.82	MS1/LS1-D1/D3-MS3-MS1	3.59
13	3,332.82	3,336.41	US1/LS3-MS3/D4-MS3/LS1-MS1/LS1	5.75
14	3,336.41	3,342.00	MS1/LS1-MS1/SD4-US1/LS3	5.59
15	3,342.00	3,348.76	MS1/LS1-SD3-D1-MS1/SD1-MS1/LS3-MS1/LS1	6.76
16	3,348.76	3,354.53	MS1/LS1-LS3-D3-MS1/LS3-MS1/LS1	5.77
17	3,354.53	3,360.46	MS1/LS1-SD1/D1-SD3/D4-MS1/D1-MS1/LS1	5.93
18	3,360.46	3,364.98	LL1-MS1/D4-MS1/SD4-MS1/LS1	4.52
19	3,364.98	3,366.86	US1/LS3-MS1/LS1-D4-LL1	1.88
20	3,366.86	3,371.28	MS1/LS1-SD3/D3-US1/LS3	4.43
21	3,371.28	3,376.26	MS1/LS1-MS1/SD1-MS1/SD2-MS1/LS1	4.98
22	3,376.26	3,380.11	MS1/SD4-LS3/D1-MS1/LS1	3.85
23	3,380.11	3,386.29	MS1-MS1/LS3-SD4/D1-LS3/D4-MS1/SD4	6.17
24	3,386.29	3,389.29	MS1/LS1-MS1/LS3-MS1/SD1-MS1-SD4-MS1/SD1-MS1/LS1	3.00
25	3,389.29	3,393.10	US1/LS3-US1/SD4-MS1/D2-MS1/SD1-MS1/LS1	3.82
26	3,393.10	3,398.47	US1-LS3/D4-MS1/LS1-D1-US1/LS3	5.37
27	3,398.47	3,404.59	MS1/LS3-LS1/SD1-SD4/D3-MS1/SD1-MS1/LS1-US1	6.12
28	3,404.59	3,407.23	MS1/SD4-SD2/D1-MS1/LS3	2.64
29	3,407.23	3,410.50	MS1/SD1-SD1/D1-MS1/SD4	3.26
30	3,410.50	3,413.06	MS1-SD2/SD3-MS1/SD1	2.56
31	3,413.06	3,416.17	MS4-D1-SD2-LS1-MS1	3.12
32	3,416.17	3,419.17	US1-SD4/D3-LS4/D1-MS4	2.99
33	3,419.17	3,421.39	US2-LS2-D1-SD1-LS1-US1	2.22
34	3,421.39	3,427.96	LL2-MS1-LS2/SD2-LS4/D1-LS2-US2	6.57
35	3,427.96	3,430.69	LL2-MS1-SD2/D1-LS1	2.73
36	3,430.69	3,434.28	LL2-MS1-SD4/D1-MS1-LL2	3.59
37	3,434.28	3,436.24	US2/SD2-US2/SD3-LL2	1.95
Average thickness				5.04

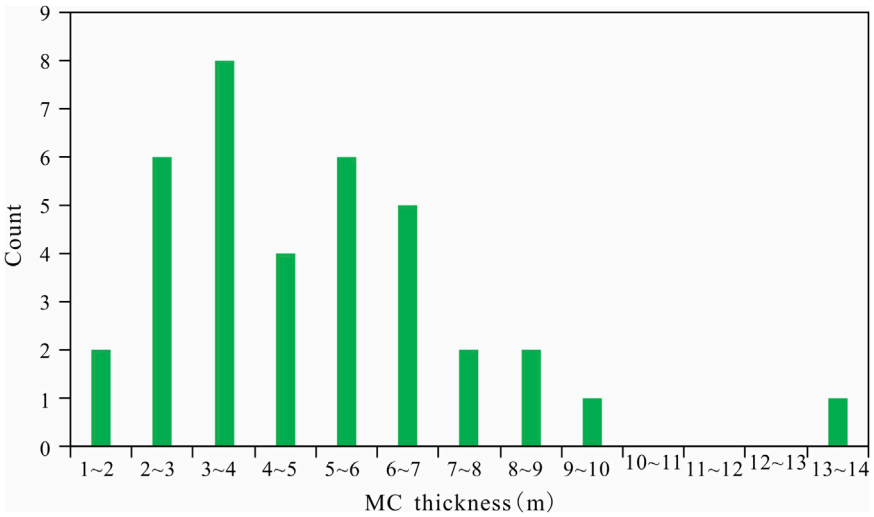

FIGURE 6
MC thickness for Es_4^u in Boxing Subsag.

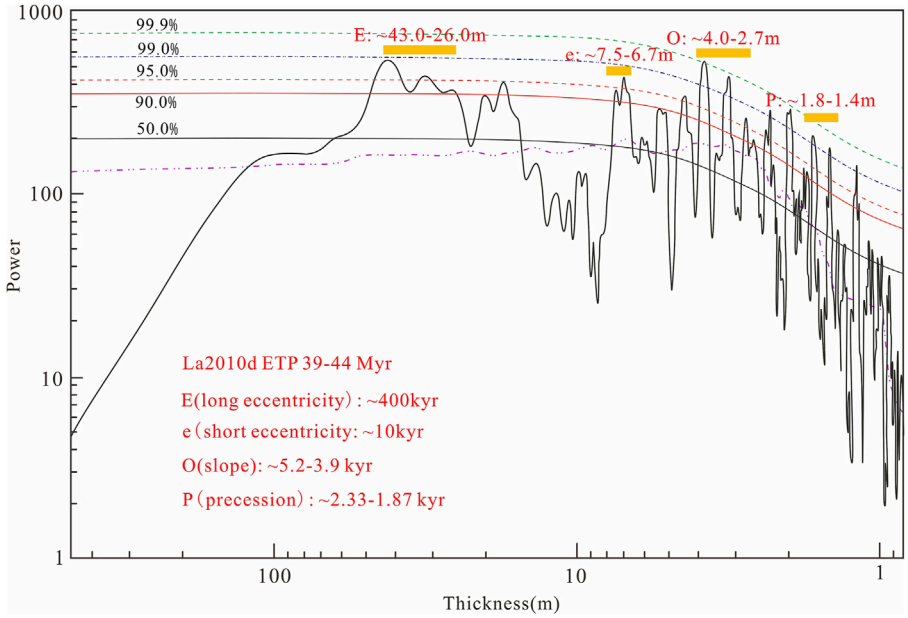

FIGURE 7
Spectral analysis of the astronomical cycle.

parameters obtained by XRF. The Th logging data of Well FY1, 3,250–3,440 m, were selected for spectral analysis after detrending using Acycle software. The existing literature indicates that the geological age of Es_4^u in the Dongying Sag is between 39 and 44 Ma (Yao et al., 2007; Liu et al., 2017; Shi et al., 2019), and La2010d is considered the most reliable astronomical solution since 54 Ma (Hilgen et al., 2010; Westerhold et al., 2012). Therefore, according to the astronomical cycle ratio (E:e:O:P = ~ 400 kyr: ~10 kyr:~5.2–3.9 kyr:~2.33–1.87 kyr) in the corresponding time of La2010d, the thickness of cycles with high confidence similar to the ratio was identified in the Es_4^u shales of Well FY1, which corresponds to E (~43–26 m), e (~7.5–6.7 m), O (~4–2.7 m), and P (~1.8–1.4 m), respectively (Figure 7). Finally, the Th log data were filtered to obtain the filtering curve of each astronomical parameter.

A comparison of the vertical variation of astronomical parameters, lithofacies, and logging response provides the findings in four aspects. First, long eccentricity changes roughly in a pattern consistent with logging curves. The maximum of long eccentricity (E) corresponds to high GR and low R, whereas the minimum of long eccentricity (E) corresponds to low GR and high R. In addition, the thickness of the lithofacies cycle obtained from the logging curve is, on average, 35 m, which falls within the range of

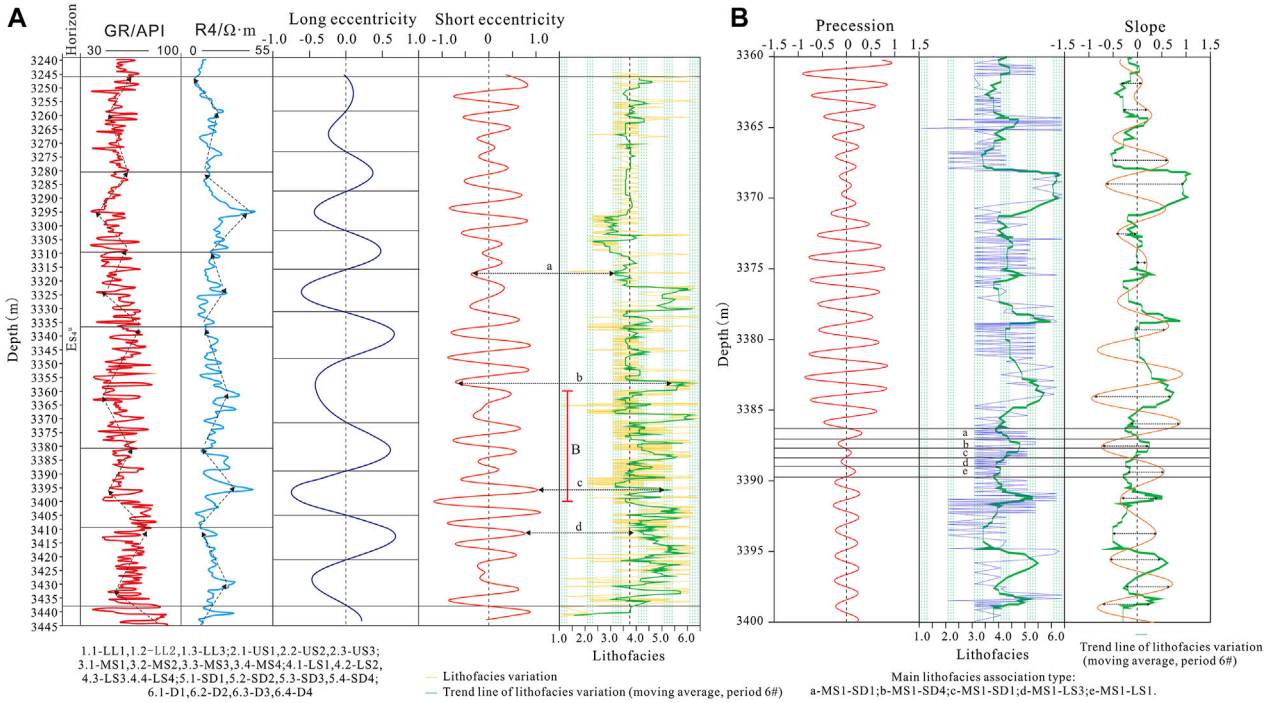

FIGURE 8
Relationship between long eccentricity, short eccentricity and lithofacies **(A)** and relationship between slope, precession and lithofacies **(B)**.

the formation thickness under the control of long eccentricity (E). Therefore, long eccentricity (E) is closely related to LC displayed by logging curves. Second, short eccentricity (e) has no evident relation to lithofacies. In Figures 8A-a, b, the trough of short eccentricity (e) corresponds to the low value and sometimes to the high value of lithofacies. In Figures 8A-c, d, the trough of short eccentricity (e) corresponds to the high value and sometimes to the low value of lithofacies. Third, the slope (O) changes in a relatively consistent pattern with lithofacies association. In Figure 8B, the maximum of the trend line of most lithofacies corresponds to the minimum of the slope (O), and the minimum of the trend line of lithofacies corresponds to the maximum of the slope (O). From the MC thickness presented by the lithofacies association, the MCs with a thickness of 3–4 m are the most developed. By contrast, the MC thickness controlled by slope (O) is approximately 2.7–4 m, proximate to the MC thickness presented by multiple lithofacies associations. Therefore, slope (O) is most related to MC. Fourth, precession (P) is well correlated to single lithofacies association. In Figures 8B-a–e, a precession (P) semi-cycle is basically composed of 1–2 SCs, and its thickness is proximate to the formation thickness (0.7–0.9 m) controlled by a half precession (P) cycle. Therefore, the precession (P) curve shows a close relationship with SC.

5.2 Control of local paleogeological conditions on lithofacies cycles

Numerous studies have shown that geochemical elements and their ratios are important parameters for paleoclimate analysis and environmental reconstruction and are considered “fingerprints” of climate and environmental evolution at multiple timescales (Croudace and Rothwell, 2015). Typically, Rb/Sr and Sr/Cu are widely used to reflect paleoclimate changes in the geological history (Fu et al., 2018; Wang et al., 2021). The paleoclimate change reflected by Rb/Sr obtained by XRF core scanning is consistent with that reflected by the chemical index of alteration (CIA) obtained by conventional XRF element testing (ICP), suggesting that Rb/Sr obtained by XRF core scanning is reliable for reconstructing the paleoclimate of fine-grained sediments (Yang et al., 2020). Generally, a high Rb/Sr value of lacustrine sediment indicates a humid and warm climate, and a low Rb/Sr value indicates a dry and hot climate. A Sr/Cu value of 1.5–7.0 indicates a warm and humid climate, and a Sr/Cu value greater than 10 indicates a dry and hot climate (Yu et al., 2021). The sediments of the continental rift basin are featured by close provenance, and the terrigenous input has an important impact on the composition and texture of lithofacies. Inert and weak migration elements (e.g., Ti and Al) are extremely sensitive to changes in dynamic conditions during material migration and are often not affected by chemical weathering and changes in redox conditions. Therefore, the degree of terrigenous input is often identified using the contents of Al and Ti. The higher the contents of Al and Ti, the more the terrigenous clastic input (Liu and Zhou, 2007; Yang et al., 2015). The abundance of Sr can be used for qualitative judgment of water salinity (Wang et al., 2016). The Rb/K can be used to distinguish the paleosalinity of the sedimentary water body. The Rb/K of normal marine shale is greater than 0.006, whereas that of fluvial sediments is less than 0.004 (Campbell and Williams, 1965). The Fe/Mn can be used to indicate the distance from shore and the ancient redox conditions, thus reflecting the

10.3389/feart.2023.1136012

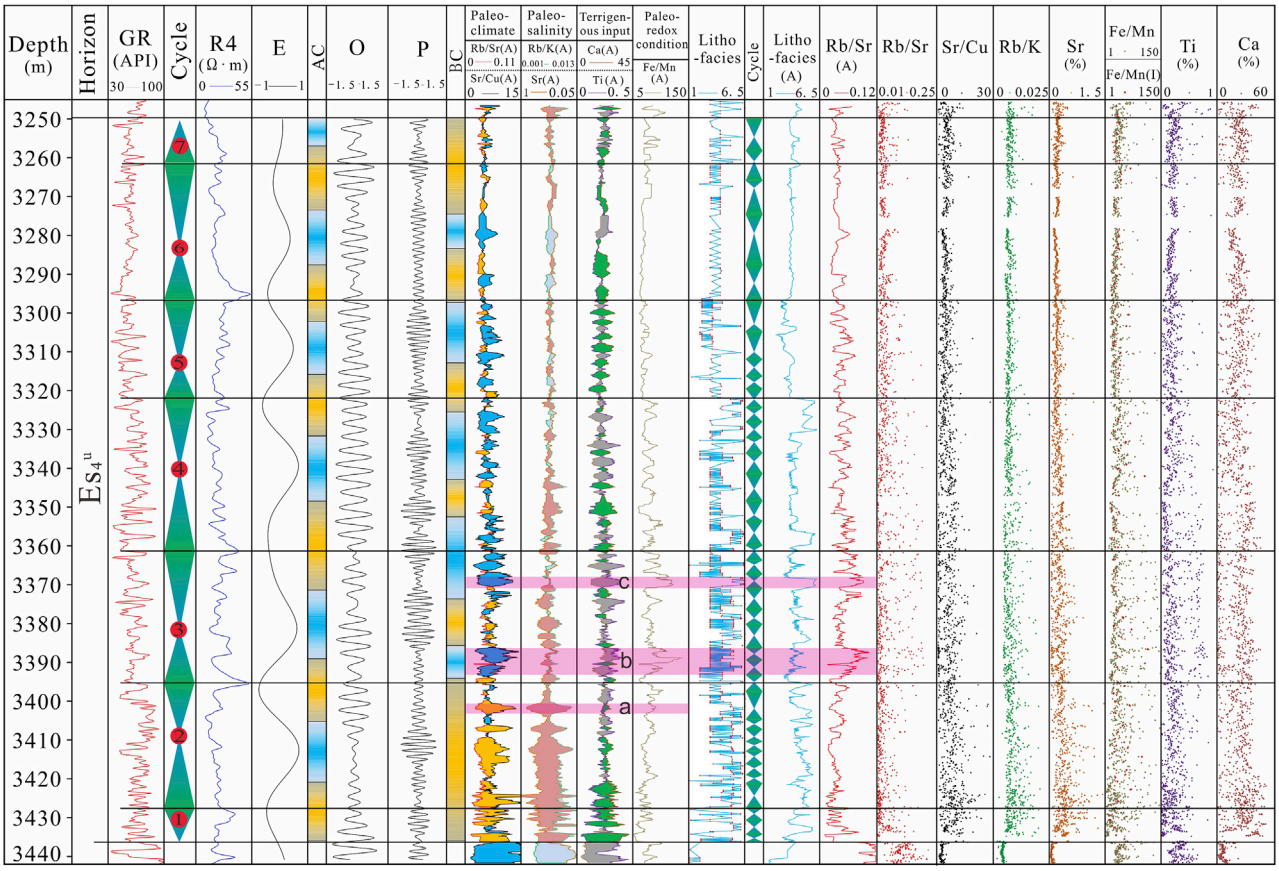

FIGURE 9
Comprehensive analysis of lithofacies cycles, astronomical parameters, and paleoenvironmental parameters [(A) means moving average, period 6#].

depth of the ancient water body at the time of deposition, and a lower Fe/Mn value suggests a deeper water body at the time of deposition and a more reduced sedimentary floor (Chen, 2008; Wang et al., 2012; Liu et al., 2019). In this study, Rb/Sr and Sr/Cu obtained by XRF core scanning are selected to analyze the paleoclimate of the Es_4^u, the Ti content is selected to analyze the characteristics of terrigenous input, the Sr content and Rb/K are selected to analyze the paleosalinity, and the Fe/Mn is selected to analyze the paleowater depth and redox conditions. The Fe/Mn determined by ICP (Fe/Mn (I) in Figure 9) was compared with the Fe/Mn obtained by XRF core scanning (Fe/Mn in Figure 9) to verify data reliability. The Fe/Mn determined by ICP completely falls within the range of the Fe/Mn ratio obtained by XRF core scanning and exhibits a consistent variation trend, proving data reliability from XRF core scanning.

There is good correspondence among the change trends of paleoclimate, paleosalinity, paleoredox conditions, and terrigenous input. For example, during the deposition of layer (Figure 9A), the paleoclimate was relatively dry, the paleosalinity was relatively high, the terrigenous input was low, the water body was evidently layered, and the sedimentary environment was prone to be reduced. When the paleoclimate was humid, the paleosalinity was relatively low, the terrigenous input was intensified, the water body was poorly layered, and the sedimentary environment was prone to oxidizing. This change law also indicates data reliability from XRF core scanning.

Previous studies have shown that, in the middle and low latitude regions of the Northern Hemisphere, when the eccentricity is near the maximum, the orbit of Earth is more elliptical, and the amplitude of precession modulated by the eccentricity increases, which jointly leads to the greater seasonal difference in this period, thus inducing intensified summer monsoon, more rainfall, and humid climate. When the eccentricity is near the minimum, the climate is dry. When the slope is near the maximum, the direct solar radiation range is shrunk toward the equator, and the middle and high latitude regions are characterized by slight changes in temperature in four seasons with a relatively dry climate. When the slope is near the minimum, the direct solar radiation range expands, and the middle and high latitude regions have four distinct seasons, with frequent water vapor transportation, more rainfall, and a relatively humid climate (Sun et al., 2017; Shi et al., 2019). The eccentricity filtering and slope curves can be used to identify the theoretical astronomical climate (AC in Figure 9) changes. The paleoclimate reflected by Rb/Sr and Sr/Cu is the actual basin climate (BC in Figure 9) change during the deposition. It is found that the astronomical climate (AC) change is very different from the actual basin climate (BC) change in a long period, and approximately 85 m strata reveal the opposite climate indications, which account for 45% of the Es_4^u strata

(186 m). Thus, it is inferred that the paleogeological conditions of the basin significantly impact the paleoclimate. When such an impact is less than the impact of the astronomical climate, the astronomical climate dominates the paleoclimate of the basin. When such an impact is greater than the impact of the astronomical climate, the basin presents a paleoclimate opposite to the astronomical climate. In Es_4^u, about 55% thickness of the strata deposition is controlled mainly by the astronomical climate, and about 45% thickness of the strata deposition is controlled mainly by the paleogeological conditions of the basin. The changes in the paleogeological conditions of the basin include the lack of summer monsoon caused by the uplift of the basin periphery, the basement decline, the rapid rise of lake level, and the expansion of the lake zone caused by the activity of the fault-controlled basin or sag.

According to the paleoclimate curve (Rb/Sr (A) in Figure 9) and the lithofacies curve (Lithofacies (A) in Figure 9), paleoclimate and lithofacies may vary synchronously and reversely. For layer b in Figure 9, the lithofacies changes in a reverse trend to the paleoclimate. For layer c in Figure 9, the lithofacies synchronously changed in a synchronous trend with the paleoclimate. Both intervals are in relatively humid paleoclimate. During the deposition of layer b, the lake level rose, the sediment supply increased, and the stratification of the water body sometimes descended owing to the inflow water, forming a cycle of lenticular laminated lithofacies alternating with continuous laminated lithofacies. During the deposition of layer c, the sediment supply increased, but the lake level was significantly higher than that for layer b, and the range of semi-deep-lake and deep-lake expanded and formed a cycle dominated by laminated lithofacies.

From the aforementioned discussion, the lithofacies cycle is evidently controlled by the paleoclimate. According to the vertical variation of Sr/Cu, the Es_4^u of Boxing Subsag was deposited under a climate that gradually transits from relatively dry at the bottom upward to relatively humid, but it was relatively humid as a whole. Under this setting, the periodic changes in long eccentricity, slope, and precession lead to the formation of different scales of the lithofacies cycle in Es_4^u. However, affected by the paleogeological conditions of the basin, the lithofacies associations within LCs and MCs are different in stacking style. However, they record the cyclical changes in the paleoclimate and paleo-lake level. SCs are repetitive vertically and record the cyclical changes in paleoclimate.

As for the shale deposits in a continental rift basin represented by the Es_4^u of Boxing Subsag, the development of lithofacies cycles was driven by the cyclicity of astronomical parameters, but it was affected by the basin paleogeological conditions, leading to significantly different lithofacies types and stacking styles within the lithofacies cycles. Therefore, the controls of the astronomical driving mechanism and the basin paleogeological conditions should be analyzed comprehensively to reveal the origin of lithofacies cycles.

5.3 Significance of the study

The study found that the shale lithofacies cycles in continental rift basin are a product of the astronomical driving mechanism and change in basin paleogeological conditions, which is different from the sedimentary cycle record of marine shale that is evidently controlled by the Milankovitch cycle and improves the understanding of the depositional environments and sedimentary processes. This finding is first proposed in the study area. Based on this finding, a new model of shale deposition can be established, the prediction of lithofacies and shale oil reservoir dessert will be easier to achieve, and the prediction accuracy will be improved. This study also presents a novel approach to analyzing and understanding the relationship between the lithofacies cycles, astronomical parameters, and the sedimentary environment, which will be applied to the study of lacustrine shales in other continental rift basins and reveal the filling process and evolution of sedimentary basins. In addition, the study idea and method can be extended to the research objects of other sedimentary types and stratigraphic horizons in the same area and adjacent area, for instance, turbidites developed in Es_3^m and beach bars developed in Es_4^l of Dongying Sag.

6 Conclusion

Through core analysis for the Es_4^u of the Boxing Subsag, 22 types of typical lithofacies are identified: three types in the lower lakeshore slope zone, three types in the upper shallow-lake slope zone, four types in the middle shallow-lake slope zone, four types in the lower shallow-lake slope zone, four types in the semi-deep-lake zone, and four types in the deep-lake zone. These lithofacies can indicate the relative position of the paleo-lake level and the characteristics of the paleoenvironment.

Three scales of the lithofacies cycle are developed in Es_4^u of the Boxing Subsag: small-scale lithofacies cycle indicated by alternate development of two lithofacies (SC), mesoscale lithofacies cycle indicated by the repetition of lithofacies associations or regular variation of multiple lithofacies (MC), and large-scale lithofacies cycle indicated by regular variation of well logging curves (LC).

The Milankovitch cycle analysis shows that the periodic change in long eccentricity is closely related to LC, the periodic change in slope is closely related to MC, and the periodic change in precession is closely related to the SC. The lithofacies cycles are evidently controlled by the paleoclimate. The periodic changes in long eccentricity, slope, and precession formed different scales of lithofacies cycles in Es_4^u of the Boxing Subsag. However, affected by the paleogeological conditions of the basin, the lithofacies associations within LCs and MCs are different in stacking style. However, they record the cyclical changes in the paleoclimate and paleo-lake level. SCs are repetitive vertically and record the cyclical changes in paleoclimate.

Data availability statement

The original contributions presented in the study are included in the article. Further inquiries can be directed to the corresponding author.

Author contributions

All authors listed have made a substantial, direct, and intellectual contribution to the work and approved it for publication.

Funding

This study was financially supported by the Natural Science Foundation of China (nos 42172153, 41802172, and 41830431), the National Science and Technology Major Project of China (no. 2017ZX05049-4), the Key Scientific and Technological Project of SINOPEC (no. KL21042), and the Key Scientific and Technological Research Project of Shengli Oilfield (no. YGK2204).

Conflict of interest

ZF was employed by the company Sinopec Shengli Oilfield Company.

The remaining authors declare that the research was conducted in the absence of any commercial or financial relationships that could be construed as a potential conflict of interest.

Publisher's note

All claims expressed in this article are solely those of the authors and do not necessarily represent those of their affiliated organizations, or those of the publisher, the editors, and the reviewers. Any product that may be evaluated in this article, or claim that may be made by its manufacturer, is not guaranteed or endorsed by the publisher.

References

Abels, H., Aziz, H., Ventra, D., and Hilgen, F. J. (2009). Orbital climate forcing in mudflat to marginal lacustrine deposits in the Miocene Teruel basin (northeast Spain). *J. Sediment. Res.* 79 (11), 831–847. doi:10.2110/jsr.2009.081

Campbell, F., and Williams, G. (1965). Chemical composition of shales of mannville Group (lower cretaceous) of central alberta, Canada. *AAPG Bull.* 49 (1), 81–87. doi:10.1306/A66334EA-16C0-11D7-8645000102C1865D

Chen, Z. (2008). Mineral elemental response to the evolution of terrestrial brine faulted basin:a case study in the paleogene of well Haoke1, dongying sag. *Acta Sedimentol. Sin.* 26 (6), 925–932. doi:10.1103/PHYSREVLETT.102.175002

Colombié, C., Schnyder, J., and Carcel, D. (2012). Shallow-water marl-limestone alternations in the late jurassic of Western France: Cycles, storm event deposits or both? *Sediment. Geol.* 271, 28–43. doi:10.1016/j.sedgeo.2012.05.010

Croudace, I., and Rothwell, R. (2015). *Micro-XRF studies of sediment cores. Developments in paleoenvironmental research*. Berlin: Springer-Verlag, 189–226.

Fu, J., Li, S., Xu, L., and Niu, X. (2018). Paleo sedimentary environmental restoration and its significance of chang 7 member of triassic Yanchang Formation in Ordos Basin, NW China. *Petroleum Explor. Dev.* 45 (6), 998–1008. doi:10.1016/S1876-3804(18)30104-6

Gale, A., Hardenbol, J., Hathway, B., Kennedy, W., Young, J., and Phansalkar, V. (2002). Global correlation of cenomanian (upper cretaceous) sequences: Evidence for milankovitch control on sea level. *Geology* 30 (4), 291–294. doi:10.1130/0091-7613(2002)030<0291:gcocuc>2.0.co;2

Gong, Y., Du, Y., Tong, J., Zhang, K., Feng, Q., Xie, S., et al. (2008). Cyclostratigraphy: The third milestone of stratigraphy in understanding time. *Earth Science (Journal China Univ. Geoences)* 33 (4), 443–457. doi:10.3321/j.issn:1000-2383.2008.04.002

Hilgen, F., Kuiper, K., and Lourens, L. (2010). Evaluation of the astronomical time scale for the Paleocene and earliest Eocene. *Earth Planet. Sci. Lett.* 300 (1-2), 139–151. doi:10.1016/j.epsl.2010.09.044

IqbalRezaee, M. R., Smith, G., and Ekundayo, J. (2021). Shale lithofacies controls on porosity and pore structure: An example from ordovician goldwyer formation, canning basin, Western Australia. *J. Nat. Gas Sci. Eng.* 89, 103888. doi:10.1016/j.jngse.2021.103888

Ito, M., Nishikawa, T., and Sugimoto, H. (1999). Tectonic control of high-frequency depositional sequences with durations shorter than milankovitch cyclicity: An example from the pleistocene paleo-tokyo bay, Japan. *Geology* 27 (8), 763–766. doi:10.1130/0091-7613(1999)027<0763:tcohfd>2.3.co;2

Kitamura, A. (1997). Responses of marine molluscs to environmental changes caused by milankovitch cycle. *Fossils* 63, 40–48. doi:10.14825/kaseki.63.0_40

Kukla, G. (2005). Saalian supercycle, mindel/riss interglacial and milankovitch's dating. *Quat. Sci. Rev.* 24 (14-15), 1573–1583. doi:10.1016/j.quascirev.2004.08.023

Li, M., Huang, C., Ogg, J., Zhang, Y., Hinnov, L., Wu, H., et al. (2019). Paleoclimate proxies for cyclostratigraphy: Comparative analysis using a lower triassic marine section in south China. *Earth Sci. Rev.* 189, 125–146. doi:10.1016/j.earscirev.2019.01.011

Liu, G., and Zhou, D. (2007). Application of micro-elements analysis in identifying sedimentary environment -taking qianjiang Formation in the jianghan basin as an example. *Petroleum Geol. Exp.* 29 (3), 307–310. doi:10.1016/S1872-5813(07)60034-6

Liu, S., Cao, Y., and Liang, C. (2019). Lithologic characteristics and sedimentary environment of fine-grained sedimentary rocks of the Paleogene in Dongying sag,Bohai Bay Basin. *J. Palaeogeogr.* 21 (3), 479–489. doi:10.7605/gdlxb.2019.03.030

Liu, Z., Huang, C., Algeo, T., Liu, H., Hao, Y., Du, X., et al. (2017). High-resolution astrochronological record for the paleocene-oligocene (66-23 Ma) from the rapidly subsiding bohai Bay Basin, northeastern China. *Palaeogeogr. Palaeoclimatol. Palaeoecol.* 510, 78–92. doi:10.1016/j.palaeo.2017.10.030

Machlus, M., Olsen, P., Christie, B., and Hemming, S. (2008). Spectral analysis of the lower eocene wilkins peak member, green river formation, Wyoming: Support for milankovitch cyclicity. *Earth Planet. Sci. Lett.* 268 (1/2), 64–75. doi:10.1016/j.epsl.2007.12.024

Olariu, C., Zhang, Z., Zhou, C., Yuan, X., Steel, R., Chen, S., et al. (2022). Conglomerate to mudstone lacustrine cycles revealed in junggar basin, northwest China: Middle permian lucaogou and jingjingzigou formations. *Mar. Petroleum Geol.* 136, 105473. doi:10.1016/j.marpetgeo.2021.105473

Ridente, D., and Lobo, F. (2014). Stratigraphic architecture and spatio-temporal variability of high-frequency (milankovitch) depositional cycles on modern continental margins: An overview. *Mar. Geol.* 352, 215–247. doi:10.1016/j.margeo.2013.10.009

RidenteTrincardi, D. F., Piva, A., and Asioli, A. (2009). The combined effect of sea level and supply during milankovitch cyclicity: Evidence from shallow-marine δ18o records and sequence architecture (adriatic margin). *Geology* 37, 1003–1006. doi:10.1130/G25730A.1

Shi, J., Jin, Z., Liu, Q., Zhang, R., and Huang, Z. (2019). Cyclostratigraphy and astronomical tuning of the middle eocene terrestrial successions in the bohai Bay Basin, eastern China. *Glob. Planet. Change* 174, 115–126. doi:10.1016/j.gloplacha.2019.01.001

Shi, J., Jin, Z., Liu, Q., and Huang, Z. (2020). Depositional process and astronomical forcing model of lacustrine fine-grained sedimentary rocks: A case study of the early paleogene in the dongying sag, bohai Bay Basin. *Mar. Petroleum Geol.* 113, 103995. doi:10.1016/j.marpetgeo.2019.08.023

Shu, Y., Lu, Y., Hu, Q., Wang, C., and Wang, Q. (2021). Geochemical, petrographic and reservoir characteristics of the transgressive systems tract of lower silurian black shale in jiaoshiba area, southwest China. *Mar. Petroleum Geol.* 129 (1), 105014. doi:10.1016/j.marpetgeo.2021.105014

Song, M. (2019). Practice and current status of shale oil exploration in Jiyang Depression. *Petroleum Geol. Recovery Effic.* 26 (1), 1–11. doi:10.13673/j.cnki.cn37-1359/te.2019.01.001

Sun, S., Liu, H., and Cao, Y. (2017). Milankovitch cycle of lacustrine deepwater fine-grained sedimentary rocks and its significance to shale oil: A case study of the upper Es4 member of well NY1 in dongying sag. *J. China Univ. Min. Technol.* 46 (4), 846–858. doi:10.13247/j.cnki.jcumt.000638

Szurlies, M. (2007). Latest permian to middle triassic cyclomagneto stratigraphy from the central European basin, Germany: Implications for the geomagnetic polarity timescale. *Earth Planet. Sci. Lett.* 261 (3/4), 602–619. doi:10.1016/j.epsl.2007.07.018

Tan, X., Jiang, Y., Li, J., Xue, W., and Li, Z. (2015). Sedimentary record and origin of high frequency cycles in the paleogene kongdian formation in the jiyang depression. *Oil Gas Geol.* 36 (1), 61–72. doi:10.11743/ogg20150108

Tian, J., Xin, X., Ma, W., Jin, H., and Wang, P. (2011). X-ray fluorescence core scanning records of chemical weathering and monsoon evolution over the past 5 Myr in the southern South China Sea. *Paleoceanography* 26 (4), 2010PA002045–17. doi:10.1029/2010PA002045

Victorien, A., Julien, B., Tobi, P., Annette, G., Bruce, A., and Simon, B. (2019). From quantitative 3d seismic stratigraphy to sequence stratigraphy: Insights into the vertical and lateral variability of shelf-margin depositional systems at different stratigraphic orders. *Mar. Petroleum Geol.* 110, 797–831. doi:10.1016/j.marpetgeo.2019.07.007

Walters, A., Meyers, S., Carroll, A., Hill, T., and Berg, M. (2020). Lacustrine cyclicity in the early eocene green river formation, uinta basin, Utah: Evidence from x-ray fluorescence core scanning. *J. Sediment. Res.* 90 (4), 429–447. doi:10.2110/jsr.2020.24

Wang, C., Liu, C., Hu, H., Mao, J., Shen, L., and Zhao, H. (2012). Sedimentary characteristics and its environmental significance of salt-bearing strata of the member 4 of paleocene shashi Formation in southern margin of jiangling depression, jianghan basin. *J. Palaeogeogr.* 14 (2), 165–175. doi:10.7605/gdlxb.2012.02.003

Wang, T., Zhu, X., Dong, Y., Yang, D., Su, B., Tan, M., et al. (2021). Signals of depositional response to the deep time paleoclimate in continental depression lakes: Insight from the Anjihaihe Formation in the northwestern Junggar Basin. *Earth Sci. Front.* 28 (1), 60–76. Available at: https://www.earthsciencefrontiers.net.cn/CN/Y2021/V28/I1/60. doi:10.13745/j.esf.sf.2020.5.8

Wang, Y., Liu, H., Song, G., Xiong, W., Zhu, D., Zhu, D., et al. (2019). Lacustrine shale fine-grained sedimentary system in jiyang depression. *Acta Pet. Sin.* 40 (4), 395–410. doi:10.7623/syxb201904002

Wang, Y., Wang, X., Song, G., Liu, H., Zhu, D., Zhu, D., et al. (2016). Genetic connection between mud shale lithofacies and shale oil enrichment in Jiyang Depression, Bohai Bay Basin. *Petroleum Explor. Dev.* 43 (5), 759–768. doi:10.1016/S1876-3804(16)30091-X

Westerhold, T., Röhl, U., and Laskar, J. (2012). Time scale controversy: Accurate orbital calibration of the early Paleogene. *Geochem. Geophys. Geosystems* 13 (6), 6–15. doi:10.1029/2012GC004096

Woo, J., Lee, H., Ozyer, C., and Rhee, C. (2021). Effect of lamination on shale reservoir properties: Case study of the montney formation, Canada. *Geofluids* 2021 (1), 1–14. doi:10.1155/2021/8853639

Wu, H., Zahng, S., Chinnov, L., Jiang, D., and Yang, T., (2014). Cyclostratigraphy and orbital tuning of the terrestrial upper santonian-lower danian in songliao basin, northeastern China. *Earth Planet. Sci. Lett.* 407, 82–95. doi:10.1016/j.epsl.2014.09.038

Yang, H., Zhao, Y., Cui, Q., Ren, W., and Li, Q. (2020). Paleoclimatic indication of x-ray fluorescence core-scanned rb/sr ratios: A case study in the zoige basin in the eastern Tibetan plateau. *Sci. China Earth Sci.* 51 (1), 80–95. doi:10.1007/s11430-020-9667-7

Yang, W., Jiang, Y., and Wang, Y. (2015). Study on shale facies sedimentary environment of lower Es3-upper Es4 in Dongying sag. *J. China Univ. Petroleum Ed. Nat. Sci.* 39 (4), 19–26. doi:10.3969/j.issn.1673-5005.2015.04.003

Yao, Y., Xu, D., Zhang, H., and Han, Y. (2007). A brief introduction to the Cenozoic astrostratigraphic time scale for the Doying Depression, Shandong. *J. Stratigr.* 31, 423–429.

Yu, H., Xu, Z., Cheng, R., Wang, L., Gao, D., Hu, X., et al. (2021). Paleoclimate evolution and elemental geochemical response during middle jurassic-early cretaceous in tectonic regime transition period in the North yellow sea basin. *Earth Sci.* 46 (3), 1100–1118.

Zhang, R., Jin, Z., Liu, Q., Li, P., Huang, Z., Shi, J., et al. (2019). Astronomical constraints on deposition of the middle triassic chang 7 lacustrine shales in the ordos basin, central China. *Palaeogeogr. Palaeoclimatol. Palaeoecol.* 528, 87–98. doi:10.1016/j.palaeo.2019.04.030

Zhang, S., Liu, H. M., Liu, Y. L., Wang, Y., Wang, M., Bao, Y., et al. (2020). Main controls and geological sweet spot types in Paleogene shale oil rich areas of the Jiyang Depression, Bohai Bay basin, China. *Mar. Petroleum Geol.* 111, 576–587. doi:10.1016/j.marpetgeo.2019.08.054